Shell-model-based investigation on level density of Xe and Ba isotopes

Jinbei Chen (陈进北) [1,2,*] Menglan Liu (刘梦兰) [1,*] Cenxi Yuan (袁岑溪) [1,†] Shengli Chen (陈胜利) [1,‡]
Noritaka Shimizu (清水则孝) [3] Xiaodong Sun (孙小东) [2] Ruirui Xu (续瑞瑞),[2] and Yuan Tian (田源) [2]

[1]*Sino-French Institute of Nuclear Engineering and Technology, Sun Yat-sen University, Zhuhai 519082, China*
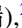[2]*China Nuclear Data Center, China Institute of Atomic Energy, P.O. Box 275(41), Beijing 102413, China*
[3]*Center for Computational Sciences, University of Tsukuba, 1-1-1 Tennodai, Tsukuba, Ibaraki 305-8577, Japan*

Nuclear level density is important for evaluating nuclear reaction processes, but its microscopic investigation is not frequently performed. The present work applies a recently developed shell-model-based method to estimate the level density of fission products $^{133-137}$Xe and $^{135-138}$Ba. The monopole-based universal interaction, V_{MU}, and the M3Y type spin-orbit interaction are combined to construct the shell-model Hamiltonian. The model space is truncated based on the binding energy of each configuration, estimated from the monopole interaction. The calculated level densities of $^{133-137}$Xe and $^{135-138}$Ba are in good agreement with available experimental data. The effects of spin-orbit and tensor forces on the nuclear level density and the shell effects in the spin distribution are discussed.

I. INTRODUCTION

Nuclear data bridges nuclear physics and nuclear engineering and technology [1]. High-precision nuclear data are crucial in developing advanced nuclear systems, such as those of actinides and fission products for the development of the generation-IV reactor [2,3]. The nuclear level density contains key information about the structure of atomic nuclei in different excited states and is closely related to key properties of nuclear reactions, the cross sections. Nuclear level density is one of the essential physical quantities in describing the nuclear reaction model. The level density of Xe and Ba isotopes, accompanied by detailed spin distribution, plays a vital role in reactor operations due to their significant fission yields. Notably, the thermal neutron capture cross section of ^{135}Xe is large [4].

However, experimental measurements of level densities are limited at high excitation energies in unstable nuclei. Most reliable experimental data concern the discrete levels at low excitation energies and the slow neutron resonance spacings at the neutron separation energy (D_0), mainly focusing on the stable nuclei [5]. The level density can be extracted from particle-γ coincidence data with the Oslo method [6–8], neutron evaporation spectra [9], etc., but are only available for dozens of nuclei [10]. Therefore, it is necessary to study the energy level densities with the help of theoretical models.

Many theoretical models of nuclear level density are phenomenological. For example, the Fermi gas model (FGM) [11] is the earliest theoretical method of level density,

where only single-particle states with equal spacings are considered. Therefore, with a simple formula and a few energy-independent parameters, the FGM is suitable for level density at high excitation energy regions of heavy-mass nuclei. On this basis, the constant temperature model (CTM) [12] and back-shifted Fermi gas model (BSFGM) [13] were developed to solve the divergence problem of the FGM at the low-energy region. Then, the generalized superfluid model (GSM) [14] considers the collective effects explicitly. Overall, the above-mentioned models successfully derive the level density near the stability line, but with large uncertainty in describing nuclei with few experimental data. The systematic study of von Egidy and Bucurescu concluded the weak agreement between all three empirical formulas and experiment results near $N = 50$ and $N = 82$ [15]. Microscopic approaches based on the nucleon-nucleon interaction and with more exact treatment on the shell effects, the pairing effects, and the spin-parity distribution are expected to be more reliable for those nuclei.

The *ab initio* theory, nuclear shell model [16,17], and mean-field approach [5] can be used to derive energy levels microscopically. But overcoming the huge computational cost has been challenging the microscopic methods. Among the above three types, the nuclear shell model has a medium computational cost and provides a detailed description of the level spectra. The shell model suggested by Mayer [18] and Jensen [19] has microscopically explained the nuclear shell structure well. It assumes the independent-particle motion of each nucleon in a mean-field potential and thus is limited in describing the many-body correlation. On this basis, the configuration-interaction shell model (CISM) [20–22] is introduced, including residual interaction and configuration mixing. Effective interaction is constructed in the truncated model space within the CISM framework, while both the

---

*These authors contributed equally to this work.

†Corresponding author: yuancx@mail.sysu.edu.cn

‡Corresponding author: chenshli23@mail.sysu.edu.cn

ground state and excited states can be derived through the diagonalization of the Hamiltonian matrix. However, constrained by the present computation ability, only low-lying levels of nuclei with a few valence nucleons can be calculated through the CISM.

Recently, a stochastic estimation method of level density in the CISM framework has been proposed by Shimizu *et al.* [23]. The level density of arbitrary spin-parity states can be derived after constructing the effective Hamiltonian, with the computational cost of the same order as that of conventional Lanczos diagonalization for low-lying levels [23]. Such a method expands the application scope of the CISM to derive the level density. But the dimension of the Hamiltonian matrix should still be constrained. In a physical view, this method will be successful only if a processable and accurate effective Hamiltonian has been constructed.

In the present work, we derive the level density of Xe and Ba isotopes in the CISM framework after discussing the truncation of model space and the construction of the effective Hamiltonian to balance the computation cost and accuracy. The present work is organized as follows. Section II introduces the theoretical methods, including the CISM framework, the stochastic estimation method, and the truncation methods. Section III validates the constructed Hamiltonian, proposes the truncation energy, and then presents the derived level densities of Xe and Ba isotopes, including the discussion on contributions from different interaction channels and the comparison of the parity and spin distributions with empirical models. Finally, a summary is given in Sec. IV.

II. MICROSCOPIC METHOD

A. Configuration-interaction shell model

The CISM framework provides a reliable microscopic basis to obtain the level density of an arbitrary spin-parity state. It usually includes three steps to solve a many-body Schrödinger equation: choosing the model space, constructing the effective Hamiltonian, and diagonalizing the Hamiltonian matrix. In practice, the shell gaps are used to divide the core, model space, and outer space. The Hamiltonian is written as two parts, the single-particle energies (SPEs) and two-body matrix elements (TBMEs).

The nuclear interaction V can be divided into the central part(V_C), spin-orbit part (V_{LS}), and tensor part (V_T), shown as

$$V = V_C + V_{LS} + V_T. \quad (1)$$

The five proton orbits between $Z = 50$ and $Z = 82$ and the 11 neutron orbits between $N = 50$ and $N = 126$ are included in the present model space to calculate the Xe and Ba isotopes. Such a model space considers the excitation crossing the $N = 82$ shell, but requires further truncation to adapt the present computation ability.

The monopole-based universal interaction, V_{MU} [24], and the M3Y type of spin-orbit interaction [25] (V_{MU}+LS) are used to construct the effective Hamiltonian in the present work. V_{MU} contains a central force in Gaussian form and a bare $\pi + \rho$ meson exchange tensor force. CISM investigations, with V_{MU}+LS mainly as the cross-shell inter-

action, were well performed in *psd* [26], *sdpf* [27], *pfsdg* regions [28], and the nearby regions of ^{132}Sn [29] and ^{208}Pb [30–32]. Recently, V_{MU}+LS was tried, as a unified interaction, for studying the excitation energies of medium-heavy nuclei around ^{132}Sn and ^{208}Pb [33,34]. Compared with V_{MU} proposed in Ref. [24], the proton-proton (neutron-neutron) central forces in the present work are enhanced by 15% (5%), following suggestions in Refs. [33,34], to further improve the calculation accuracy of low-lying excitation energies of medium-heavy nuclei. The constructed Hamiltonian is examined in Sec. III along with the discussion of the corresponding results.

CISM codes usually apply the Lanczos method to derive a few lowest-lying levels [35]. In the present work, we apply the shell-model code KSHELL [36] to calculate the discrete low-lying levels and a revised version of KSHELL [23], which is based on the stochastic estimation method without diagonalization for level-density calculations.

B. Stochastic estimation method

The CISM can, in principle, calculate all levels strictly based on the determined model space and the corresponding effective Hamiltonian but suffers from the excessive requirement of computational effort. The computational resource required by the Lanczos method is proportional to the required number of states, thus easily exceeds the present computational limit in the level-density study. Nowadays, the computational limitation of the shell-model diagonalization is around 10^{11} matrix dimensions, so only a few states are considered. Therefore, a method other than diagonalization is required for estimating nuclear level density.

The present work employs the stochastic estimation method introduced in Ref. [23]. According to the residue theorem, the number of levels in an energy range can be counted with the contour integral. More clearly, one has

$$\mu_k = \frac{1}{2\pi i} \sum_j \oint_{\Gamma_k} \frac{1}{z - \lambda_j}, \quad (2)$$

where μ_k, λ_j, and Γ_k represent the numbers of energy levels, the eigenvalues of the Hamiltonian, and the contour integrals on the complex plane, respectively.

Because the Hamiltonian matrix (H) is real symmetric, it can be deduced that

$$\mu_k = \frac{1}{2\pi i} \sum_j \oint_{\Gamma_k} \frac{1}{z - \lambda_j} = \frac{1}{2\pi i} \oint_{\Gamma_k} dz \mathrm{tr}((z - H)^{-1}). \quad (3)$$

Then the integral is numerically derived with discretization. Taking z_j^k as the integral points and w_j the corresponding weights, one has

$$\mu_k \approx \sum_j w_j \mathrm{tr}\left((z_j^k - H)^{-1}\right). \quad (4)$$

The calculation of the trace of the matrix can be simplified by employing a stochastic method with random vectors. In addition, the complex orthogonal conjugate gradient (COCG) method [37] and the shifted Krylov subspace method [38] are adopted in numerical calculation to avoid reorthogonalization,
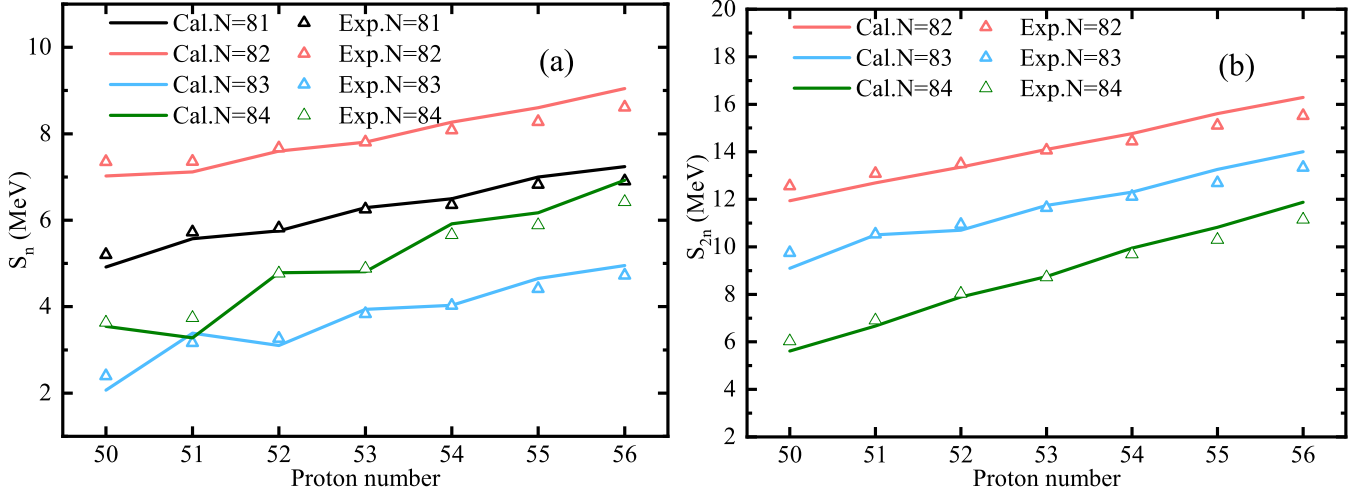
FIG. 1. (a) One- and (b) two-neutron separation energies of nuclei around ^{132}Sn. The theoretical results are calculated by CISM with V_{MU}+LS interaction, while the experimental data are from AME2020 [45].

which reduces the amount of calculation. The implementation of the code combined the shell-model code KSHELL and the eigenvalue solver library z-Pares [39]. We apply the code proposed in Ref. [23] on the Tianhe-2 supercomputer.

C. Monopole-based truncation

To calculate the Xe and Ba isotopes within the current computational capability, the present model space, which includes five proton orbits and 11 neutron orbits, needs to be further truncated. For this purpose, the nucleon-pair approximation is a commonly used truncation approach [40] in the $A \approx 130$ region. The present work proposes another truncation method based on the monopole interaction.

Effective single particle energy (ESPE) [22,41] provides a reference for shell structure. It can be written as [42,43]

$$\varepsilon_j = \varepsilon_j^{\mathrm{c}} + \sum_j V_{jj'} \langle \psi | \widehat{N}_{j'} | \psi \rangle, \tag{5}$$

where $\varepsilon_j^{\mathrm{c}}$ is the single-particle energy of the j orbit relative to the core, $\langle \psi | \widehat{N}_{j'} | \psi \rangle$ denotes the neutron occupation number of the j' orbit, and $V_{jj'}$ is the monopole interaction between two orbits, whose formula can be found in Refs. [42,43]. Based on the ESPE, the shell-model energy relative to the core energy of each single-particle configuration (E_{SC}) is estimated by Eq. (6):

$$
\begin{aligned}
E_{SC} &= \sum_{j,j'} \varepsilon_j \langle \psi | \widehat{N}_{j'} | \psi \rangle \\
&= \sum_j \langle \psi | \widehat{N}_j | \psi \rangle \varepsilon_j^{\mathrm{c}} + \sum_{jj'} \frac{V_{jj'}}{2} \langle \psi | \widehat{N}_j | \psi \rangle \langle \psi | \widehat{N}_j | \psi \rangle.
\end{aligned}
\tag{6}
$$

Only single-particle configurations with estimated E_{SC} below the truncation energy are included in the truncated model space. It is supposed that the configurations with a much higher E_{SC} would not significantly contribute to the level density below that truncation energy [44]. Such a truncation method efficiently reduces the computational dimension while the computational accuracy is largely maintained.

III. RESULTS AND DISCUSSION

A. Discrete level

In the present work, the Hamiltonian is constructed for nuclei in the region "north" of ^{132}Sn. The TBMEs are first derived with V_{MU}+LS interaction. The SPEs are fixed with the observed excited energies of ^{131,133}Sn and ^{133}Sb [46]. Neutron excitation across the $N = 82$ shell gap is not included in the CISM calculations of this subsection.

The separation energy is ideal for examining the evolution of shell structure when adding valence protons and/or neutrons. Figure 1 presents the one and two neutron separation energies (S_{2n}) for $50 \leqslant Z \leqslant 56$ nuclei around $N = 82$, where the calculations nicely agree with the experimental observations and indicate a reasonable shell structure. Except that the S_n of ^{135}Sb measured to be 0.57 MeV larger than that of ^{134}Sb, is not precisely reproduced in the present work. Separating one neutron in ^{134}Sb, where the valence proton and neutron occupy the $\pi 0g_{7/2}$ and $\nu 1f_{7/2}$ orbits, respectively, means the breaking of a proton-neutron pair. On the contrary, separating one neutron in ^{135}Sb will lead to forming a proton-neutron pair. The proton-neutron correlation appearing in ^{134,135}Sb may be slightly stronger described by the present interaction.

Figure 1(b) shows the S_{2n} values of $N = 82$–84 isotones, which reflect more clearly the single-particle-level spacings by including the pair correlation. The S_{2n} value increases linearly as the proton number grows from the magic number 50. The present interaction well describes the increase of S_{2n} per proton. Generally, the deviations between observed and calculated separation energies are acceptable, with a root-mean-square (rms) error of S_n (S_{2n}) valuing 0.25 MeV (0.43 MeV).

The low-lying excitation spectra of several Sn isotopes, $N = 82$ isotones, and nearby nuclei in the "north" ^{132}Sn region are calculated and compared with the experimental data to examine the Hamiltonian further, as shown in Figs. 2–5. The excitation spectra are well reproduced, while the rms deviation is around 0.2 MeV between the present
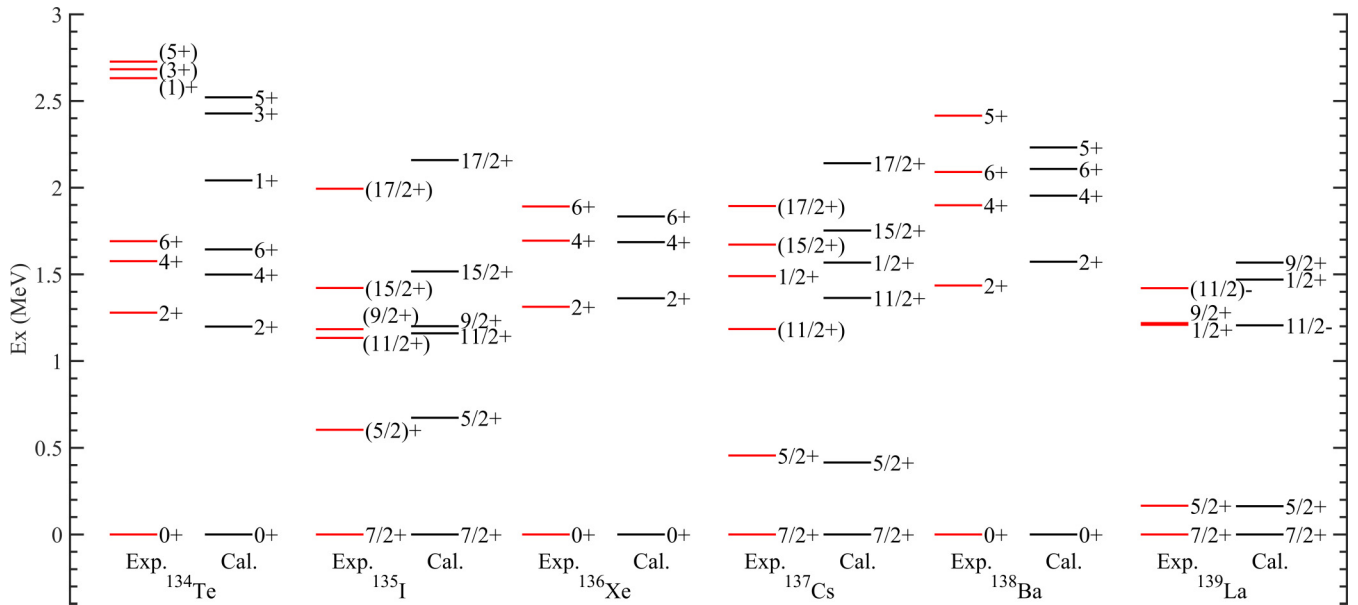
FIG. 2. Excitation spectra of $N = 82$ isotones. The theoretical results are calculated by CISM with the $V_{MU}+LS$ interaction, while the experimental data are from NNDC [46].

calculated levels and the National Nuclear Data Center (NNDC) data [46].

As shown in Fig. 2, the experimental excitation energies of $N = 82$ isotones are well reproduced, suggesting that the proton-proton interaction is reasonable. When the proton number increases, the 2_1^+, 4_1^+, and 6_1^+ states have higher excitation energies while the $5/2_1^+$ state has a lower one. The former may relate to the shape-deformation evolution resulting from collective motions [47]. The latter indicates the reduction of the shell gap between $\pi 0g_{7/2}$ and $\pi 1d_{5/2}$ when more protons occupy $\pi 0g_{7/2}$. The present interaction well reproduces the two evolution cases. In addition, theoretical

ESPEs of $N = 82$ isotones in the present work roughly favor the persistence of the $N = 82$ shell closure from Sn to Ba, which was shown to remain until the Sr isotope in the other direction [48,49].

Results of the Sn isotope are shown in Fig. 3. The nice agreement between calculations and observations validates the neutron-neutron interaction both beyond and below the $N = 82$ shell gap. The excitation energies of the 2_1^+ states in ^{128,130}Sn are significantly higher than those in ^{134,136}Sn, which reveals the different systematics between $N < 82$ nuclei and $N > 82$ nuclei. Such differences have been well reproduced with the same interaction $V_{MU}+LS$. It should be noticed that
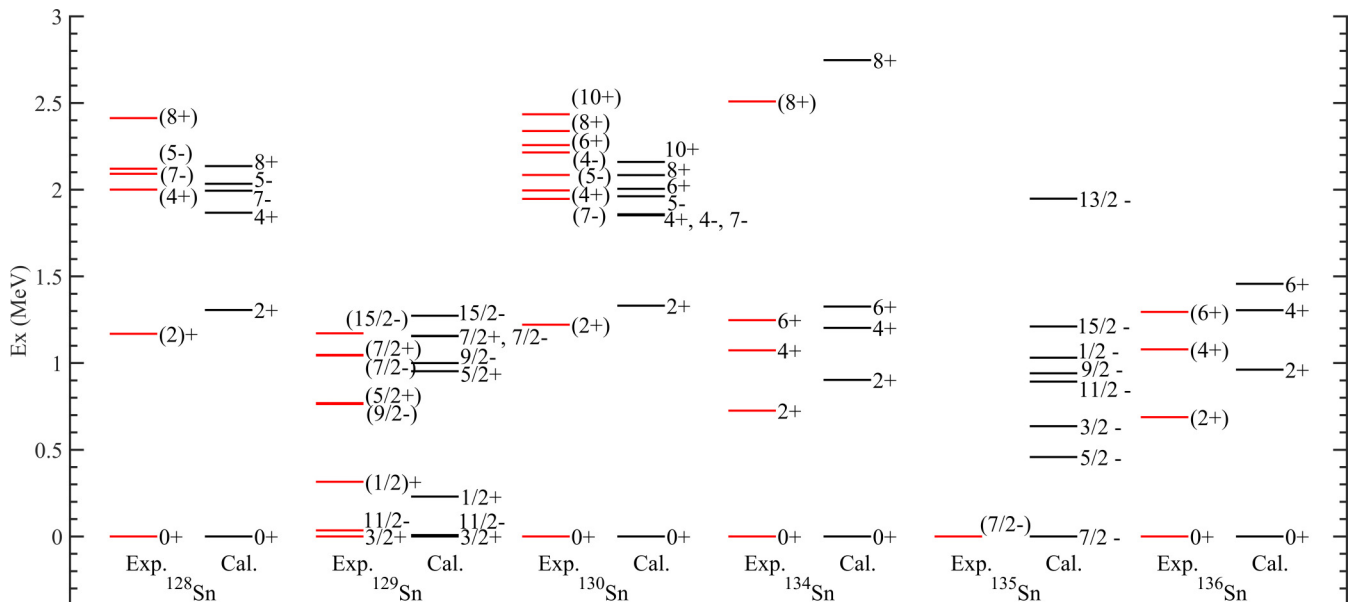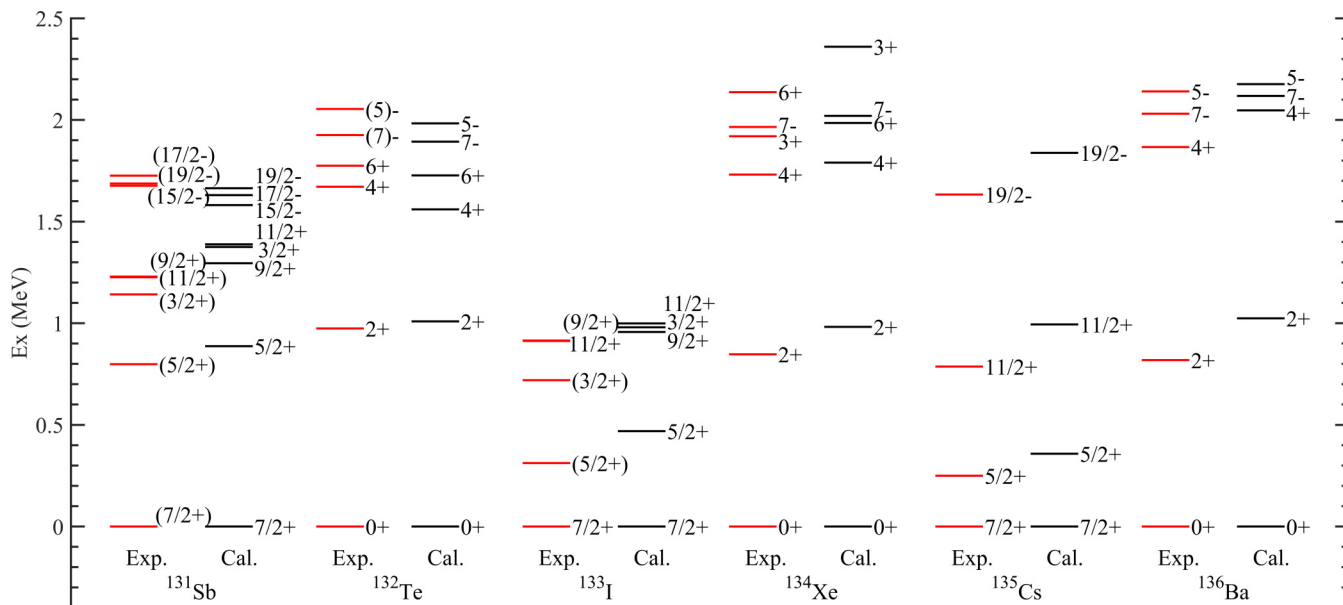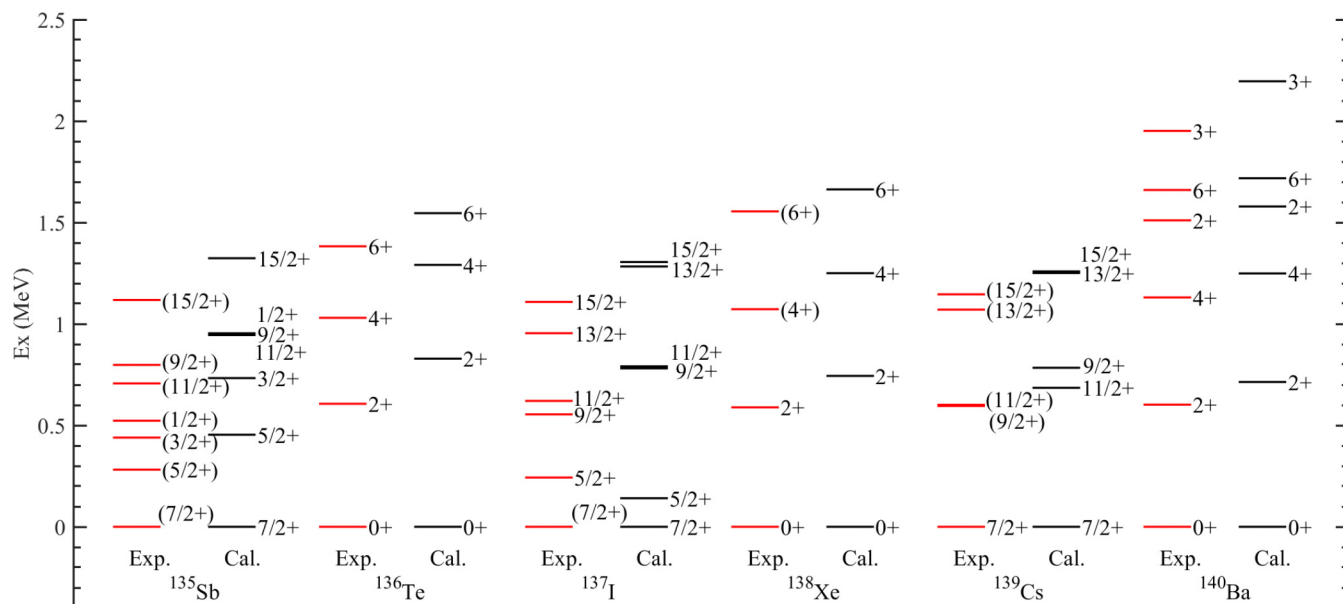

FIG. 3. The same as Fig. 2, but for Sn isotopes.

FIG. 4. The same as Fig. 2, but for $N = 80$ isotones.

only ground-state information of the r-process nucleus ^{135}Sn has been experimentally given [50]. The low-lying levels predicted by the present interaction agree with some existing interactions. For example, the predicted $3/2_1^-$ and $1/2_1^-$ states in ^{135}Sn by three interactions shown in Ref. [50] are all around 0.6 MeV and 1.0 MeV. In addition, the present level spectrum of ^{135}Sn is rather similar to the one predicted by the neutron-neutron interaction based on the CD-Bonn renormalized G matrix in Ref. [29], where the deviations of the calculated levels of ^{134,136,138}Sn from the experimental data are normally less than 0.1 MeV. Moreover, the calculated 6_1^+, 4_1^+, and 4_2^+ (not shown in Fig. 3) states in ^{136}Sn have close excitation

energies, and the calculated $B(E2, 6_1^+ \rightarrow 4_1^+)$ value of ^{136}Sn is smaller than that of ^{134}Sn, which is consistent with the studies interpreting the 6_1^+ isomer in ^{136}Sn with mixed seniority [29,51].

Excitation spectra of $N = 80$ and $N = 84$ isotones are shown in Figs. 4 and 5, respectively. For those nuclei, both protons and neutrons are included in the model space. In general, the present Hamiltonian is reasonable for both the northeast and northwest vicinity of ^{132}Sn. Compared with the results of semimagic nuclei, the measured ratios $R_{4/2} = E(4_1^+)/E(2_1^+)$ of the even-mass nuclei shown in Figs. 4 and 5 are closer to 2, which symbolizes the vibrational structure

FIG. 5. The same as Fig. 2, but for $N = 84$ isotones.

[47]. Meanwhile, the evolution of the $\pi 1d_{5/2} - \pi 0g_{7/2}$ gap can be seen in $N = 80$ and $N = 84$ isotones, as explicated in the $N = 82$ case. The present calculations generally interpreted those transition tendencies, while the data indicating the details of evolution, such as the $R_{4/2}$ ratio, can be used to improve the proposed effective interaction further.

There are some other powerful CISM interactions for the ^{132}Sn nearby region. For example, the interactions based on the extended pairing plus quadrupole-quadrupole force with monopole correction (EPQQM) were constructed by Wang *et al.* to discuss the nuclei in the "south" ^{132}Sn [48,49,52–54] and "north" ^{132}Sn [55]. The pairing plus quadrupole plus multipole interaction (and its improved version) has been used for the $A \approx 130$ region [56,57]. The realistic CD-Bonn potential is also commonly used for constructing the interactions in the "southeast" ^{132}Sn [29] and in the region "northwest" of ^{132}Sn (*jj55pna*) [57,58].

However, the existing interactions rarely include the core excitation of ^{132}Sn. Actually, the first core-excitation states of ^{132}Sn and ^{133}Sb are nearly 4 MeV. Therefore, for the states lower than 3 MeV discussed in this subsection, the interactions excluding the neutron excitation across the $N = 82$ shell gap are suitable, which reasonably considered the current computational ability. The work in Ref. [55] considered two extra neutron orbits ($\nu 1f_{7/2}$ and $\nu 2p_{3/2}$) above the $N = 82$ shell and well interpreted the core-excited states in $^{131-133}$Sb. As the orbits of $\nu 2p_{3/2}$, $\nu 0h_{11/2}$, and $\nu 0g_{9/2}$ are close to each other, all the orbits below the $N = 126$ shell gap should be included to calculate the level density in Xe and Ba isotopes up to 10 MeV.

This subsection has shown that the interaction V_{MU}+LS can both describe the $N \geqslant 82$ and $N < 82$ regions, well reproducing the observed separation energies and low-lying energy levels. V_{MU}+LS has been successfully used as cross-shell excitation in various regions in previous works. Thus, it can be concluded that the present interaction, based on V_{MU}+LS in large model space, would be suitable for calculating the level density in Xe and Ba isotopes up to 10 MeV.

B. Truncation energy

The M-scheme dimensions of the Xe and Ba isotopes at various truncation energies are displayed in Fig. 6. It can be seen that none of the $^{134-138}$Ba isotopes can be calculated without truncation within the current computational ability. Truncation energy should be introduced to make the calculations practicable.

The required computational dimension rapidly decreases as the truncation energy declines. However, the lower truncation energy with fewer configurations may lead to worse accuracy. Figure 7 presents the level density results of the Xe and Ba isotopes at truncation energies of 5, 10, and 15 MeV. The four figures for different nuclei result in similar conclusions. First of all, the truncation energy of 5 MeV is too low to estimate the level density appropriately. The calculations with 5 MeV are almost reasonable for the level density below 7 MeV but can hardly derive the levels at higher energy. It is easy to understand because states at higher energy should have configurations estimated with higher excitation energy.
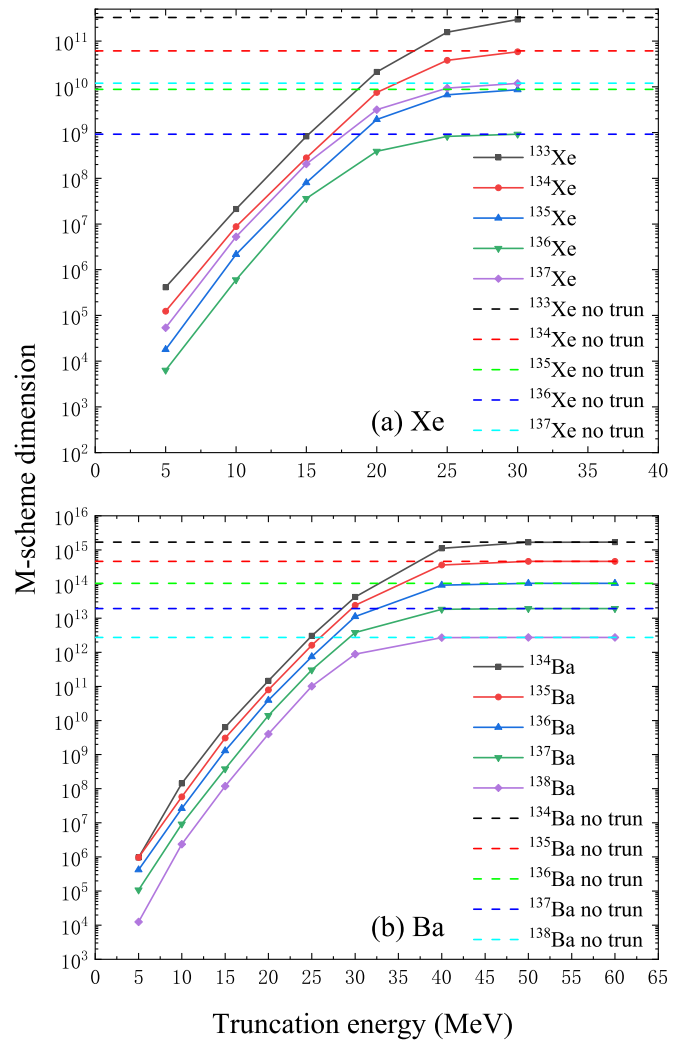

FIG. 6. Computational dimension of Xe (a) and Ba (b) isotopes at different truncation energy. The dashed line represents the results without truncation (no trun).

Meanwhile, the present truncation approach is verified because the level density results converge with increasing truncation energy. The results have a reasonable agreement between the two truncation energies, 10 MeV and 15 MeV. Therefore, the model space with a truncation energy of 10 MeV is sufficient to calculate the level density, at least for the energy range of 0–12 MeV. The following discussions concentrate more on level density below 10 MeV. Thus, the truncation energy of 10 MeV is used.

C. Level density

After validating the effective interaction and determining the truncation energy, the present work calculated the level density of $^{133-137}$Xe and $^{134-138}$Ba below 10 MeV with the revised version of KSHELL. The contribution of each component of the nuclear interaction is also investigated by removing the spin-orbit interaction (woLS), tensor interaction (woT), and both of them (woLST) in the Hamiltonian TBMEs. The level density results are shown in Figs. 8 and 9.
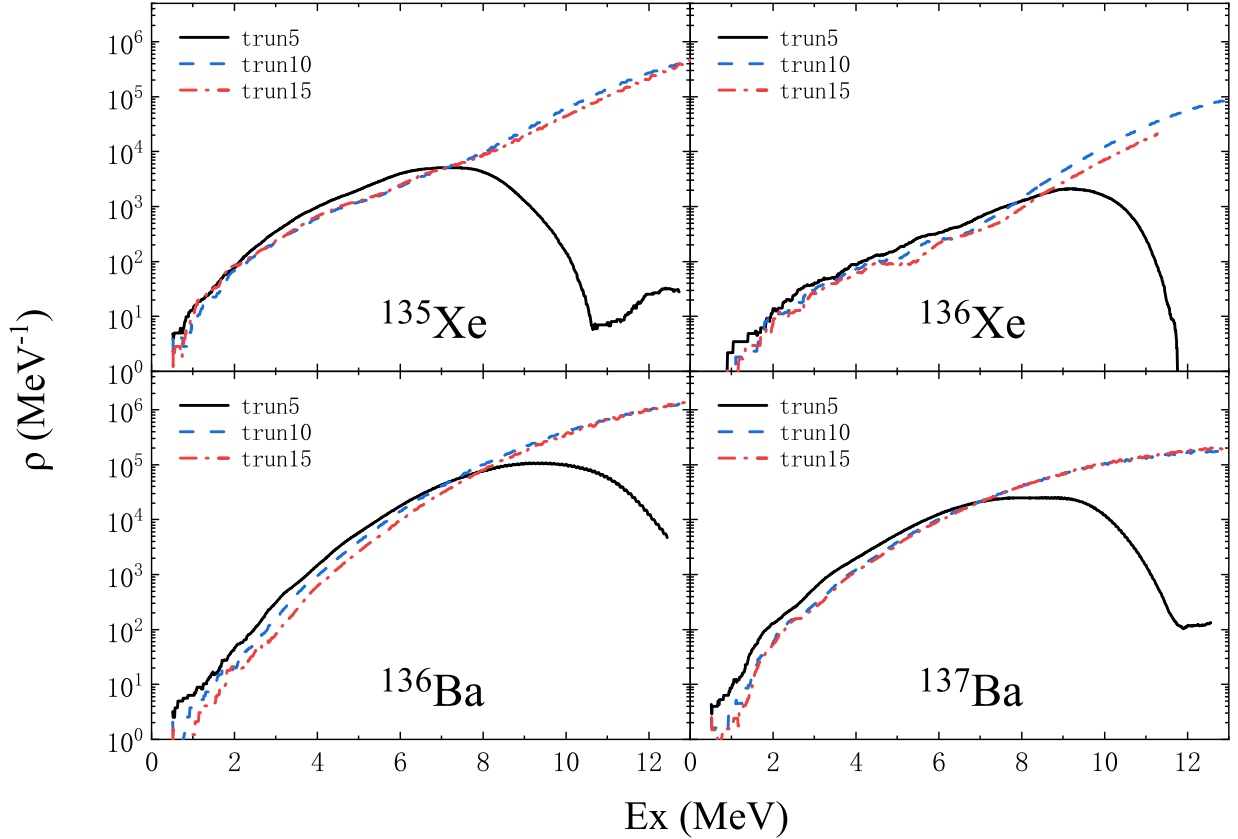
FIG. 7. Level densities for isotopes $^{135-136}$Xe and $^{136-137}$Ba, calculated with truncation energies of 5, 10, and 15 MeV.

The experimental neutron resonance spacings at neutron separation energy provide reliable experimental level-density data $\rho(S_n)$ [5,15]. The experimental data for reference in Figs. 8 and 9 are obtained based on the work of Egidy and Bucurescu [15], where the level-density data were restricted to a certain spin interval. To compare the experimental and calculated total level densities, one should introduce the spin distribution function. The spin cut-off parameter is estimated by fitting the calculated total level densities shown in Figs. 8 and 9 with the BSFGM formula [59]. For comparison, Table I displays the calculated and experimental partial level densities at S_n.

TABLE I. Comparison of the calculated and experimental partial level density at S_n for Xe and Ba isotopes.

Nucleus	$J\pi$	S_n (MeV)	This work (MeV^{-1})	HFB [60] (MeV^{-1})	Egidy [15] (MeV^{-1})
^{133}Xe	1/2+	6.434	506	611	665(210)
^{135}Xe	1/2+	6.364	61	461	313(115)
^{137}Xe	1/2+	4.026	10	46	39(18)
^{135}Ba	1/2+	6.972	1544	1390	1350(130)
^{136}Ba	1-2+	9.108	8210	44200	12500(1900)
^{137}Ba	1/2+	6.906	257	849	413(41)
^{138}Ba	1-2+	8.612	222	4090	1925(370)

The calculated level densities for ^{133,137}Xe and $^{135-137}$Ba isotopes are well consistent with the experimental data. The level densities at neutron excitation energies of 6.4 MeV for ^{135}Xe and 8.6 MeV for ^{138}Ba are smaller than the experimental value. The description of level density may demand more proton and/or neutron cross-shell excitation at high excitation energy in nuclei at or close to the $N = 82$ shell.

One should notice that the difference by a factor of 10 is not rare for the theoretical deviation on D_0 or $\rho(S_n)$. A significant part of calculated $\rho(S_n)$ by the empirical formulas has a deviation by a factor of near or larger than 2 from the experimental values in Ref. [15]. Those formulas have the worst agreement near $N = 50$ and $N = 82$ because of the insufficient consideration of shell effects. Within the framework of the Hartree-Fock-Bogoliubov (HFB) plus combinatorial method, the interactions BSK9 and BSK13 give, respectively, a rms factor (f_{rms}) of 4.9 and 2.13 for 295 experimental D_0 values [5]. Here, f_{rms} of N_n nuclei is defined as

$$f_{\text{rms}} = \exp\left(\frac{1}{N_n} \sum_{i=1}^{N_n} \ln^2 \frac{D_{0,i}^{\text{th}}}{D_{0,i}^{\text{exp}}}\right)^{1/2}. \quad (7)$$

The large disagreement of BSK9 owes to the significant pairing effect at S_n.

In a global view, the level density of both Xe and Ba isotopes decreases when approaching the $N = 82$ closed shell.
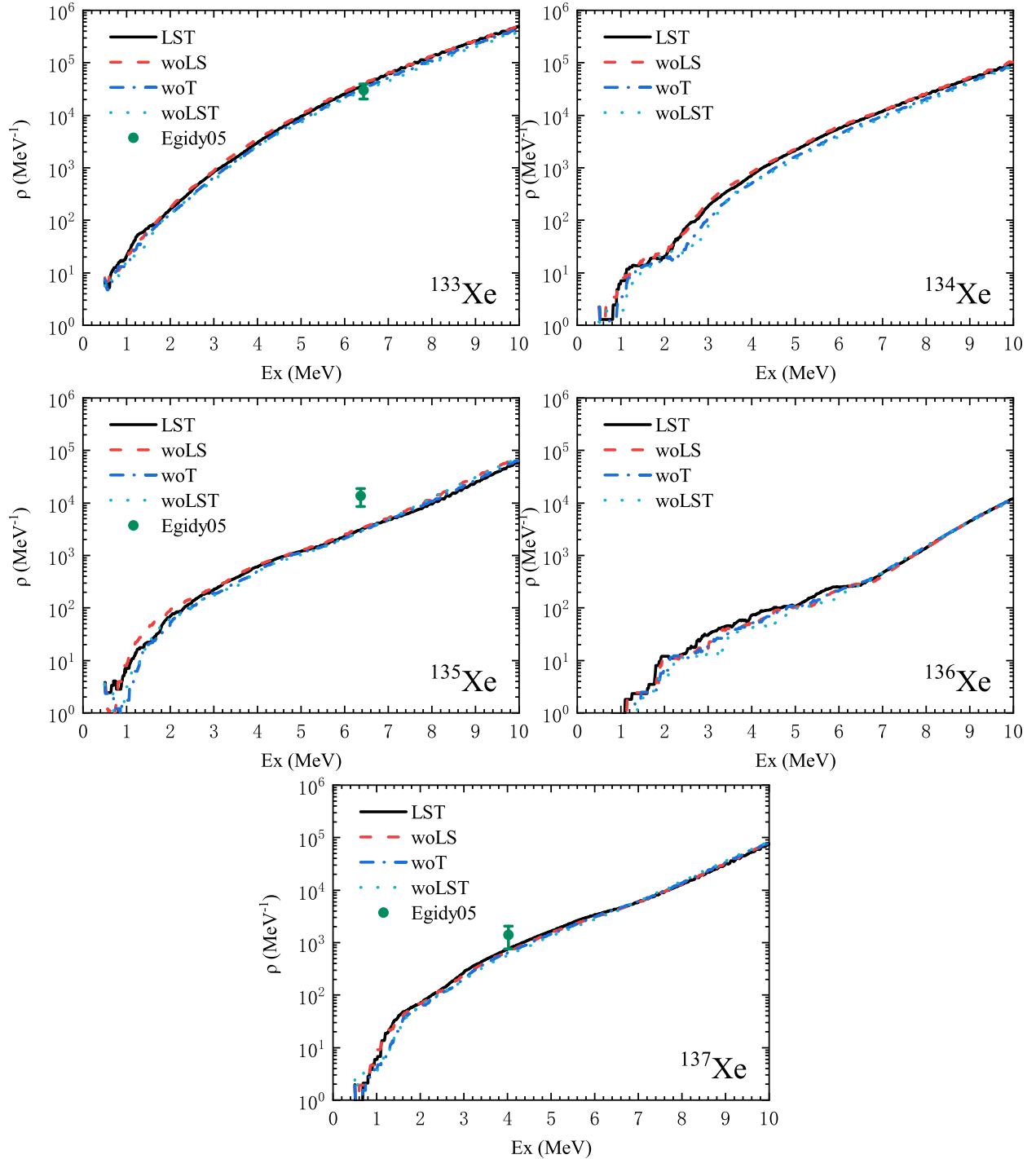
FIG. 8. Level densities for isotopes $^{133-137}$Xe with different effective interactions. "LST" is the original interaction, while "woLS", "woT", and "woLST" represent, respectively, the interactions without the spin-orbit force, tensor force, or both of them. Experimental value at neutron separation energy (labelled with "Egidy05") is derived from Ref. [15].

This phenomenon is consistent with the shell structure of atomic nuclei.

The other important type of available experimental data for level density is the discrete levels at low excitation energy. To further benchmark our calculations, we show the cumulative number of levels at a lower energy range of 0–6 MeV in Figs. 10 and 11. Here, numbers of the observed discrete levels derived from the Reference Input Parameter Library (RIPL-3) [59], and theoretical results by the CTM with parameters recommended in RIPL-3, are drawn for comparison. It should be noticed that $N_{\max}$ is the level above which the experimental cumulative number of discrete levels is not complete.
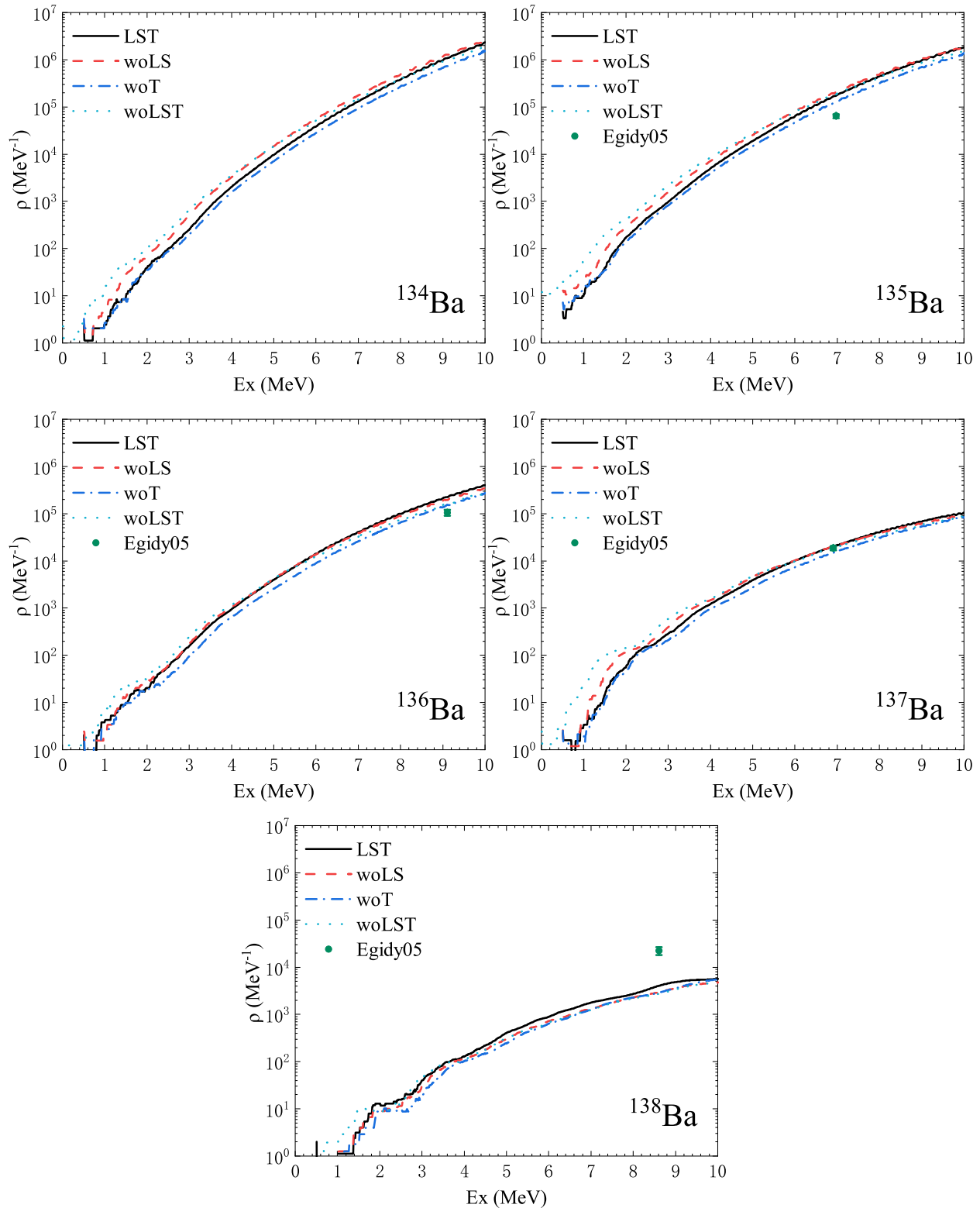
FIG. 9. The same as Fig. 8, but for isotopes $^{134-138}$Ba.

A nice agreement between the present results and the RIPL-3 reference data can be found for the cumulative number of levels below the N_{max} level. As for the case above the N_{max}, the RIPL-3 curve no longer satisfies the exponential linear increase with increasing excitation energy, because many energy levels have not been observed. For instance, experimental studies on high-spin states of Xe and Ba isotopes are in progress [57,61]. Meanwhile, the cumulative number of levels in the present calculation maintains exponential linear growth at high excitation energies, which is more reasonable.
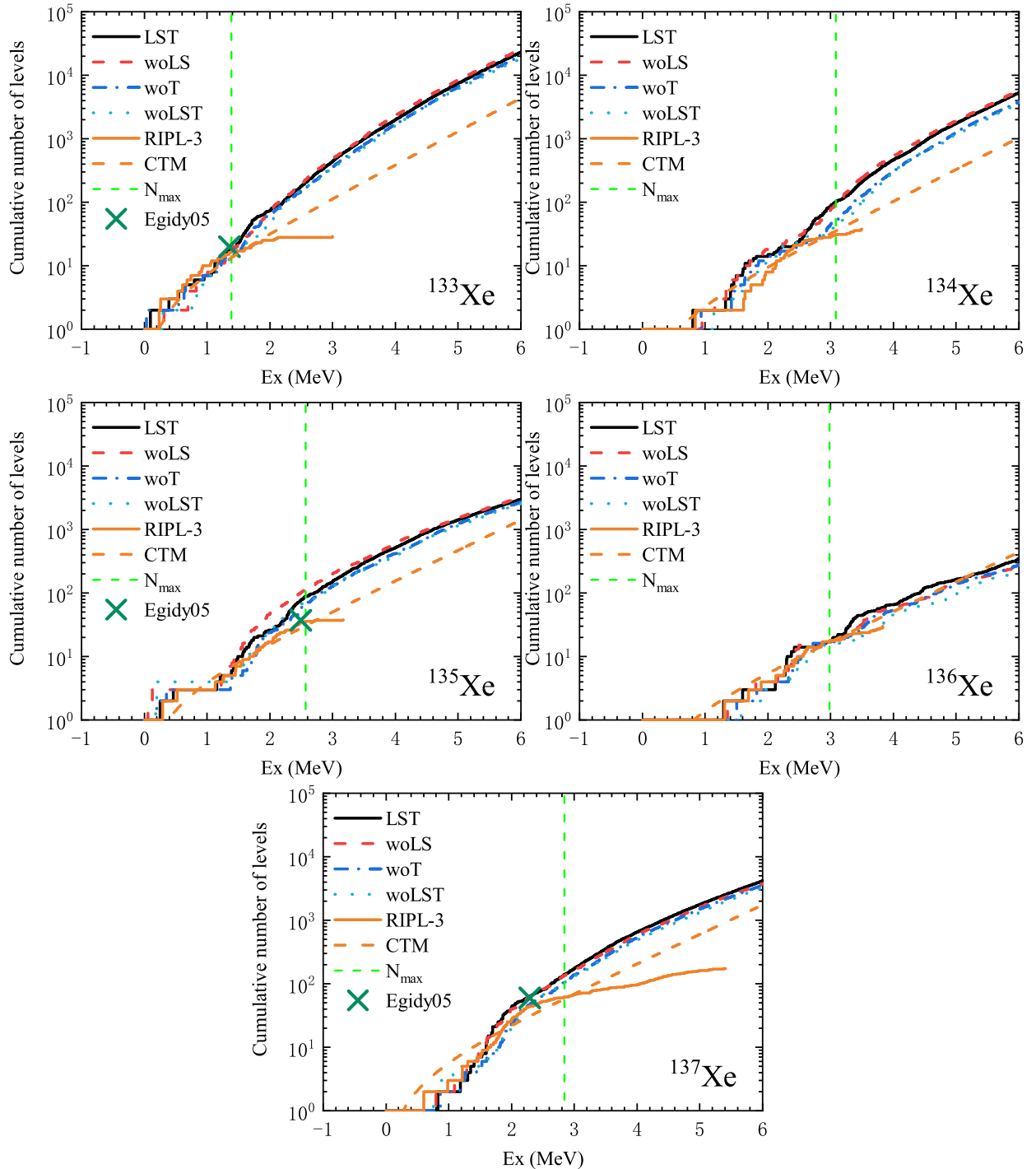
FIG. 10. Cumulative number of levels for isotopes $^{133-137}$Xe calculated with different effective interactions–LST, woLS, woT, and woLST. The data set "RIPL-3" is the experimental data provided by Reference Input Parameter Library (RIPL-3), with "N_{max}" the number of levels constituting a complete level scheme. "CTM" is theoretical data of CTM using parameters of RIPL-3. "Egidy05" is experimental data based on Ref. [15].

Though CTM is believed to provide a more reasonable description in low excitation energy than other usual phenomenological models [62], it still underestimates the level density of $A = 130$–150 nuclei at neutron resonance [15]. On the one hand, the pairing effect becomes less significant at higher energy. Thus more levels than the prediction of CTM exist. On the other hand, the shell structure evolves with

valance particles occupying higher orbits [63]. The tensor force favors the reduction of shell gaps at high excitation energy, further leading to dense levels. Therefore, the cumulative number of levels calculated by CTM and CISM are in nice agreement below N_{max}. But the present CISM calculation, which provides a microscopic description of the nuclear structure, predicts a higher level density above N_{max} than CTM.
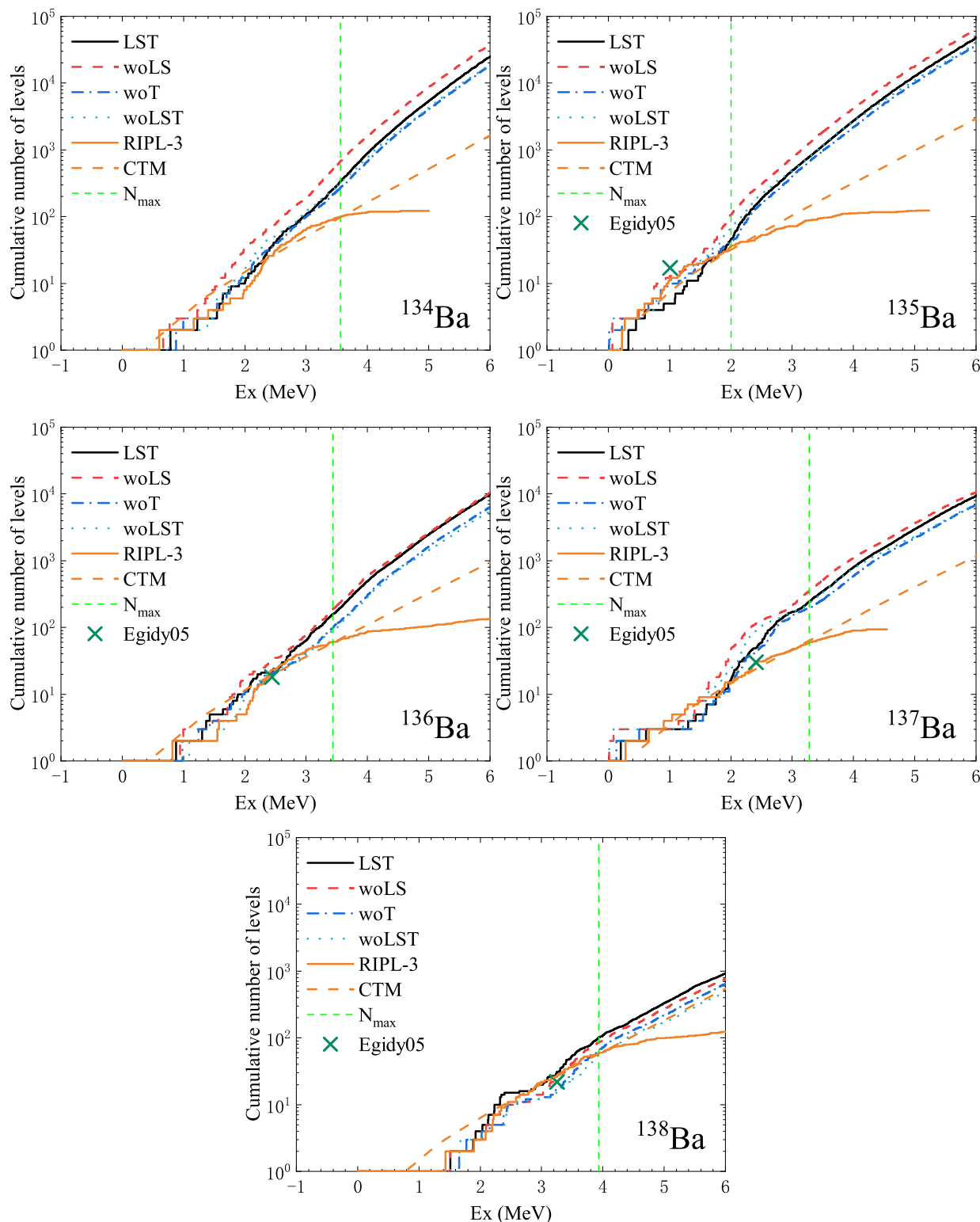
FIG. 11. The same as Fig. 10, but for isotopes $^{134-138}$Ba.

The level densities of even-mass isotopes, including ^{134,136}Xe and ^{134,138}Ba, show a sudden leap at 0.8–1.2 MeV, 1.8–2.0 MeV, 1.0–1.4 MeV, and 1.2–2.0 MeV, respectively. The development of these results is similar to the step structure of ^{118,119}Sn presented in Ref. [64], whose bumps are

produced with pair breaking of neutrons. The neutron pairing gap of ^{134,136}Xe and ^{134,138}Ba are, respectively, 1.10 MeV, 2.03 MeV, 1.25 MeV, and 1.94 MeV [46]. One can notice that the excitation energies of leaps correspond well to the neutron pairing energies of each isotope, which indicates that
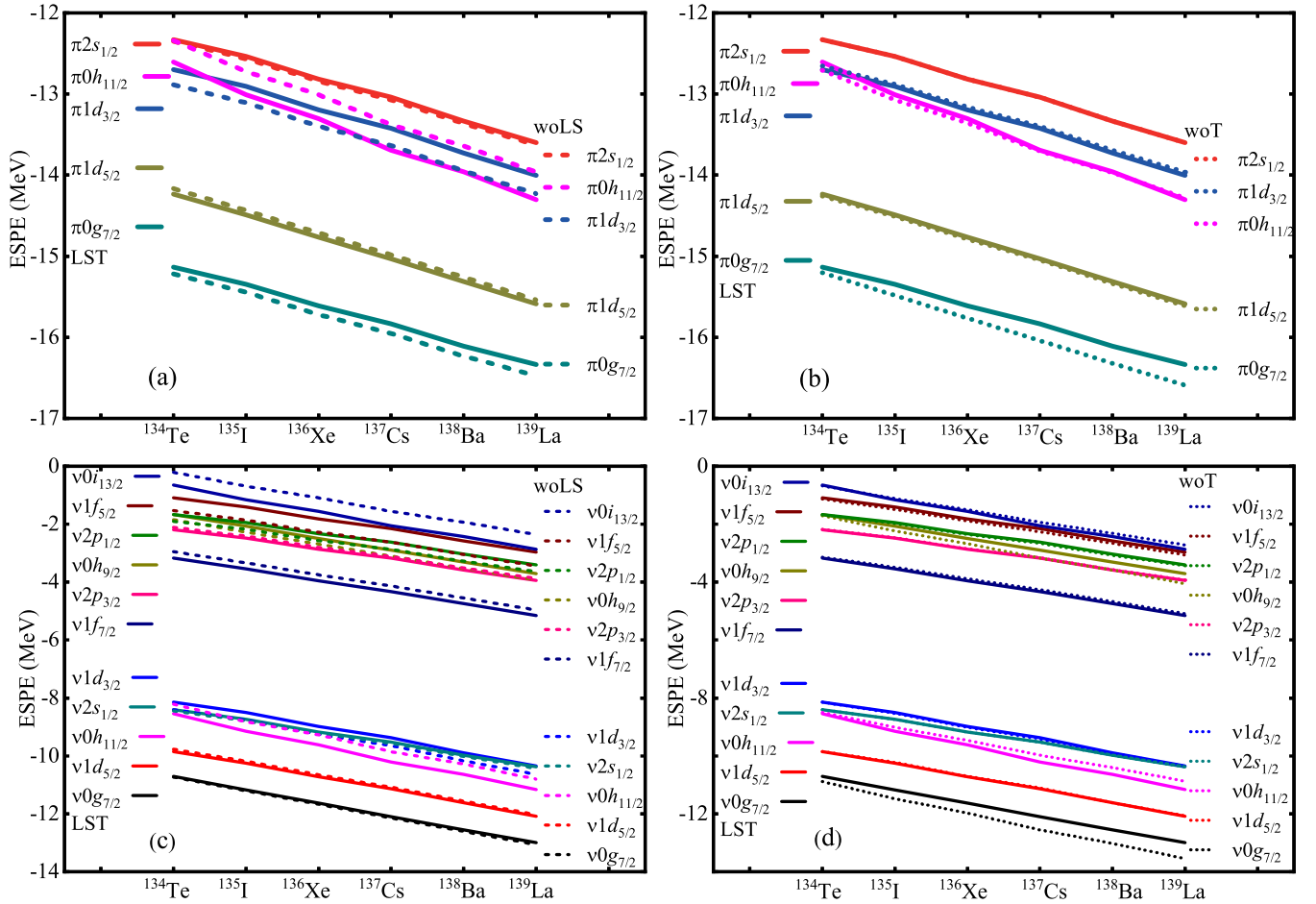
FIG. 12. ESPEs in $N = 82$ isotones of (a) proton orbits calculated with/without the spin-orbit part in the TBMEs; (b) proton orbits calculated with/without the tensor part in the TBMEs; (c) neutron orbits calculated with/without the spin-orbit part in the TBMEs; (d) neutron orbits calculated with/without the tensor part in the TBMEs.

pair breaking is the main reason for the step structure [65,66]. Breaking of Cooper pairs plays an important role in increasing level densities, especially for low excited states [67]. Besides, the leap is kept in woLS, woT, and woLST results, further validating that its origin is more like a pairing interaction.

It is of great interest to further discuss the effects of spin-orbit and tensor forces on the level density. As shown in Figs. 8–11, the level densities from the three modified interactions all maintain a similar order of magnitude to the original one, which means that the removal of spin-orbit interaction, tensor interaction, or both of them has caused a limited effect on the level density. The woLS results are slightly larger (smaller) than the LST ones in nuclei below (at or beyond) $N = 82$ shell. Because the $N = 82$ shell originates from the spin-orbit splitting, it is reasonable that removing spin-orbit interaction enhances (inhibits) the excitation below (beyond) the shell. One should note that the present woLS results only remove the spin-orbit force in the model space, while its contribution from the core still exists.

The ESPEs of the $N = 82$ nuclei calculated with and without spin-orbit interactions are shown in Figs. 12(a) and 12(c). It can be seen that the spin-orbit force influences the shell gaps and the relative orders of the neutron orbits. The inclusion of

the spin-orbit force in the TBMEs enlarges the splitting of all the orbit pairs with the same orbit angular momenta: $\nu 1f_{5/2}$ and $\nu 1f_{7/2}$, $\nu 2p_{1/2}$ and $\nu 2p_{3/2}$, $\nu 1d_{3/2}$ and $\nu 1d_{5/2}$, $\nu 0h_{9/2}$ and $\nu 0h_{11/2}$, and $\pi 1d_{3/2}$ and $\pi 1d_{5/2}$. The average enlargement resulting from the inclusion of the spin-orbit force is 0.66 MeV in the gap between the pair $\nu 1f_{5/2}$ and $\nu 1f_{7/2}$. And the average gap between the pair $\nu 2p_{1/2}$ and $\nu 2p_{3/2}$ is enhanced 131% after including the spin-orbit force. The spin-orbit coupling results in the downshift of $\nu 0i_{13/2}$ and the upshift of $\nu 1f_{5/2}$. Thus, the local density at the level of $\nu 0i_{13/2}$ would decrease after removing the spin-orbit force. On the other hand, the levels would aggregate at $\nu 2s_{1/2}$ without the spin-orbit force because the $\nu 1d_{3/2}$ orbit is pulled down while the $\nu 0h_{11/2}$ orbit is pushed up. Finally, the $N = 82$ shell gap, which is mainly caused by the spin-orbit force of the core, is slightly reduced when including the spin-orbit force in the model space.

It can be clearly seen that the same variation of ESPEs appears in the proton part. The related orders of $\pi 1d_{3/2}$ and $\pi 0h_{11/2}$ become inverse for $Z \geqslant 53$ after adding the spin-orbit force. On the whole, local nuclear level density slightly varies because of spin-orbit splitting.

The woT results are generally smaller than the LST ones, which indicates that the tensor interaction increases the level

density. It can be seen from Figs. 12(b) and 12(d) that, after removing the tensor force, the $\pi 0g_{7/2}$, $\nu 0g_{7/2}$, $\nu 2s_{1/2}$, and $\nu 0h_{9/2}$ orbits are relatively shifted, while the left orbits nearly keep unchanged. The ESPE values of the $\pi 0g_{7/2}$ and $\nu 0g_{7/2}$ orbits, which are the lowest-lying proton and neutron orbits, are reduced if removing the tensor force. Therefore, it requires more energy for particle excitation. The level density becomes smaller.

Besides, even though both ^{136}Xe and ^{138}Ba are $N = 82$ isotones, differences in level density can be observed. One reason is that the ESPEs and their gaps vary with proton number in the $N = 82$ isotones. For the $N = 82$ isotones beyond ^{132}Sn, valence protons mainly add to $\pi 0g_{7/2}$ orbit. Its tensor interaction attracts (repulses) neutron $1f_{7/2}$ ($1d_{3/2}$) orbit, which reduces the $N = 82$ shell and enhances the cross-shell excitations. From ^{134}Te to ^{135}I, the attractive force pulls down the $\nu 0h_{11/2}$ orbit and causes the orbit inverse of $\nu 0h_{11/2}$ and $\nu 1d_{3/2}$. Shell-gap reduction due to the tensor force will equally appear when nucleons are excited to higher orbits in a specific nucleus.

Removing the two noncentral forces together can be considered a superposition result of removing the two forces separately. Generally, the spin-orbit force shows a more complex contribution, while the tensor force has a bigger contribution to the ESPEs relative to the lowest orbits. The woLST results are close to the woLS results, except for the evident shift of the $\pi 0g_{7/2}$ and $\nu 0g_{7/2}$ orbits.

D. Parity and spin distribution

The previous sections mainly focus on the total level density or cumulative number of levels at given excitation energies. However, it is the partial level density that is primarily derived from the experimental resonance data. The present CISM method has a notable advantage in directly calculating the level density for a specific spin and parity, making it convenient to compare theoretical and experimental partial level densities, as shown in Table I. Additionally, the spin distribution is relevant to the angular distribution of compound nuclear reactions and the isomeric ratios [69], which is vital for the Hauser-Feshbach calculations [70]. Thus, it is necessary to investigate the calculated parity and spin distribution of the level density, and further compare them with empirical formulas.

The parity ratio at a given excitation energy π_{Ex} is defined as the share of positive-parity levels in the total levels of an energy interval [68], as shown in Eq. (8),

$$\pi_{E_x} = \frac{\rho(E_x, +)}{\rho(E_x, +) + \rho(E_x, -)}, \tag{8}$$

where $\rho(E_x, +)$ and $\rho(E_x, +)$ represent the density of levels of positive and negative parities, respectively. At high excitation energies, the parity ratio typically approaches 0.5 [12,68], making it reasonable to disregard parity dependence [15,72]. At low excitation energies, one parity can dominate in limited intervals, as evidenced by the positive parity of the lowest-lying levels in even-even nuclei. Odd-even effects should be considered at low excitation energies [68]. For instance, the parity ratio approaches 0.5 more rapidly in the odd-mass Xe
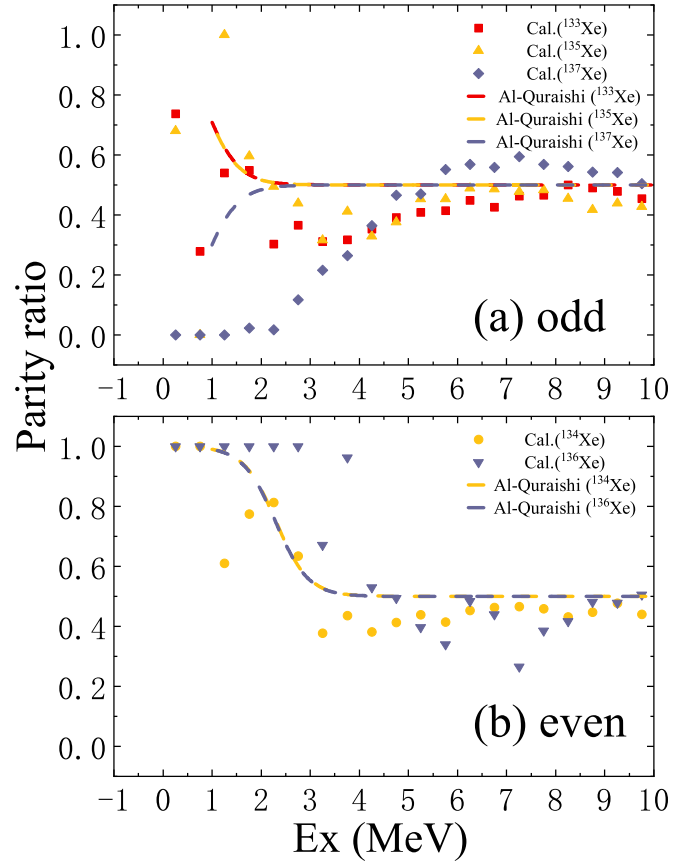

FIG. 13. Comparison of the calculated parity ratios for $^{133-137}$Xe in the present work and those in the work of Al-Quraishi *et al.* [68].

isotopes than in the even-mass ones. As illustrated in Fig. 13, our calculations generally support these findings, aligning with Ref. [68].

The spin distribution is much more complicated due to more possibilities. Whereas, a Gaussian distribution [12] is generally used in the phenomenological models, as written in the formula

$$R_F(J, \sigma) = \frac{2J + 1}{2\sigma^2} \exp\left[-\frac{\left(J + \frac{1}{2}\right)^2}{2\sigma^2}\right] \tag{9}$$

with σ the spin cut-off parameter.

Besides, systematic studies on the spin distribution function [73] suggested that the odd-even spin staggering exists in the spin distribution of even-even nuclei at low excitation energy (around 1–3 MeV). In such cases, the spin distribution formula was modified with a staggering parameter:

$$R_{\text{Fee}}(J, \sigma) = R_F(J, \sigma)(1 + x), \tag{10}$$

where x equals to $+1.02(9)$ for zero spin value, $+0.227(14)$ for other even spin values, and $-0.227(14)$ for odd spin. References [72,73] validated Eqs. (9) and (10) after fitting the experimental level-density data of more than 300 nuclei with both BSFGM and CTM.

Figure 14 shows the normalized spin distributions in ^{133,134,136}Xe at different excitation-energy intervals calculated by the present CISM method. The spin cut-off parameters are
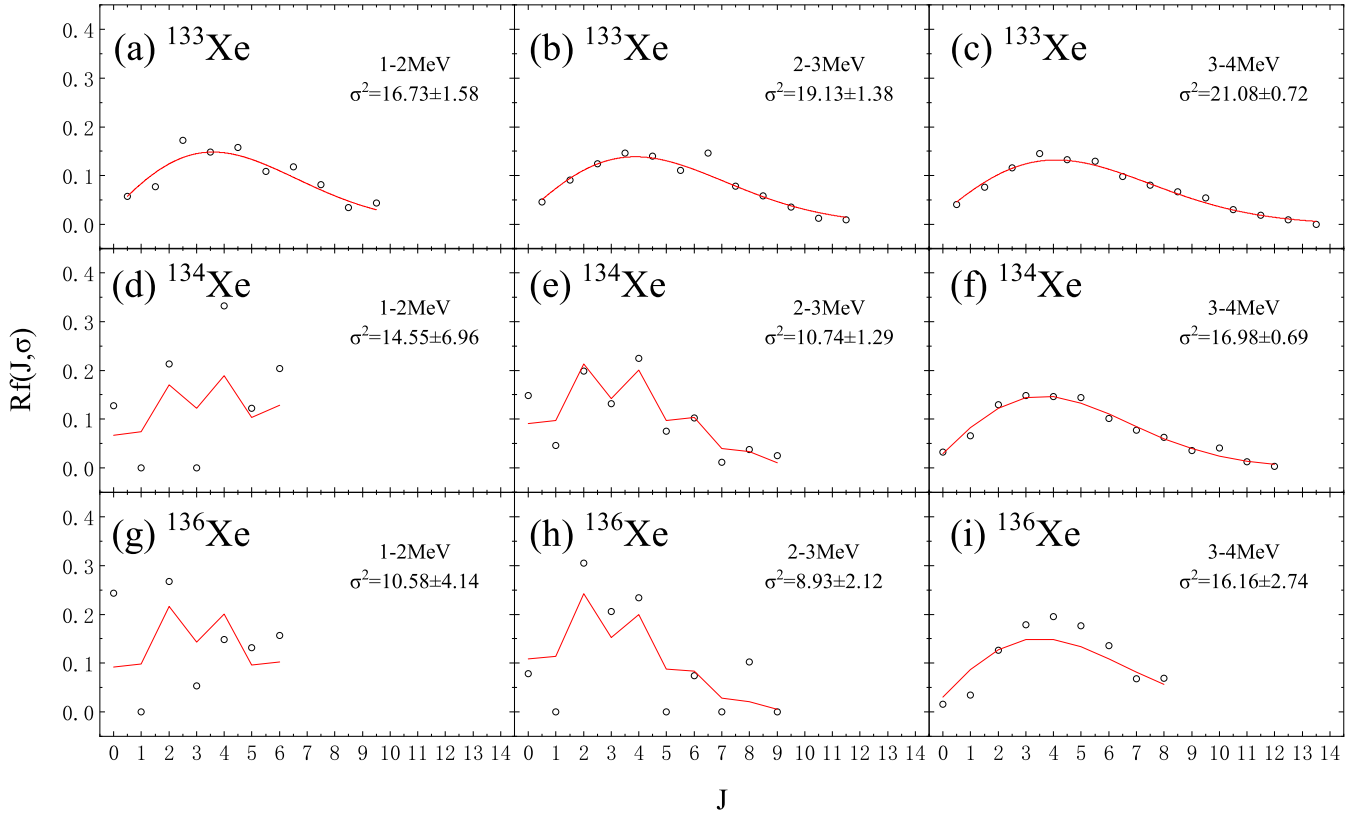
FIG. 14. Spin distribution in ^{133,134,136}Xe calculated by the present method. The spin cut-off parameters are derived from Eq. (9) (for all cases), with modifications from Eq. (10) [only for (d), (e), (g), and (h)]. The circles and the red lines represent, respectively, the calculated and the fitted results.

derived by fitting the calculated spin distribution with Eq. (9), with modifications from Eq. (10) for ^{134,136}Xe at 1–3 MeV.

As shown in Fig. 14, the spin distribution of level density in even-even nuclei exhibits a staggering structure at 1–3 MeV. The states with even spin are systematically more dense than the others, and the number of spin-zero states is especially large in even-even nuclei. It is consistent with the conclusion that the staggering parameters should be extra introduced to describe the low-energy spin distribution in even-even nuclei. And as the excitation energy rises (up to 3–4 MeV), this staggered configuration vanishes, allowing Eq. (9) to capture the spin distribution of even-even nuclei accurately. For other types of nuclei, no significant odd-even staggering has been found even at 1–2 MeV, as in the case of ^{133}Xe shown in Fig. 14. The results are overall in agreement with Ref. [73], where the spin odd-even staggering of 1–3 MeV even-even nuclei was interpreted with the pairing correlation. One should also notice that the states are less discrete and sparse at low excitation energy, which may lead to both the incompleteness of the experimental level scheme and the inapplicability of statistical methods.

The calculated spin distributions of Xe isotopes at 3–10 MeV were fitted with Eq. (9). It is helpful to compare the spin cut-off parameters derived from the partial level density of the present study with previous systematic studies. In Ref. [69], the spin cut-off parameters calculated with four different models and those experimentally derived are compared. It points

out the deficiency of the rigid-body model at low excitation energies and the good agreement of different models at high excitation energy. Figure 15 presents the spin cut-off parameters for $^{133-137}$Xe at 4, 6, and 8 MeV calculated in the present study, along with those presented in Ref. [69]. The calculated σ^2 are in reasonable agreement with the experimental and other theoretical results. More precisely, the present results are distributed between the data of rigid-body model [69] and that derived with Ref. [72] (labeled "Egidy09").

To further investigate the dependence of the spin cut-off parameters on the excitation energy and the mass number, the derived spin cut-off parameters at different excitation energies are shown in Fig. 16.

On the one hand, the spin cut-off parameter generally grows with increasing excitation energy. At high excitation energy, the σ^2 value is proportional to $\sqrt{E_x}$ for $^{133-135}$Xe, which is consistent with both the rigid-body model [69] and the semiempirical formula proposed by Ericson [12]:

$$\sigma^2 = \frac{6}{\pi^2}\sqrt{E_x a}\langle m^2 \rangle, \tag{11}$$

where a represents the level density parameter, and $\langle m^2 \rangle$ denotes the square average of the angular momentum projection on Z axis for single-article states at the Fermi level.

On the other hand, the fitted σ^2 value of Xe isotopes for high excitation energy (higher than 5 MeV) decreases when the neutron number approaches 82, which shows an obvious
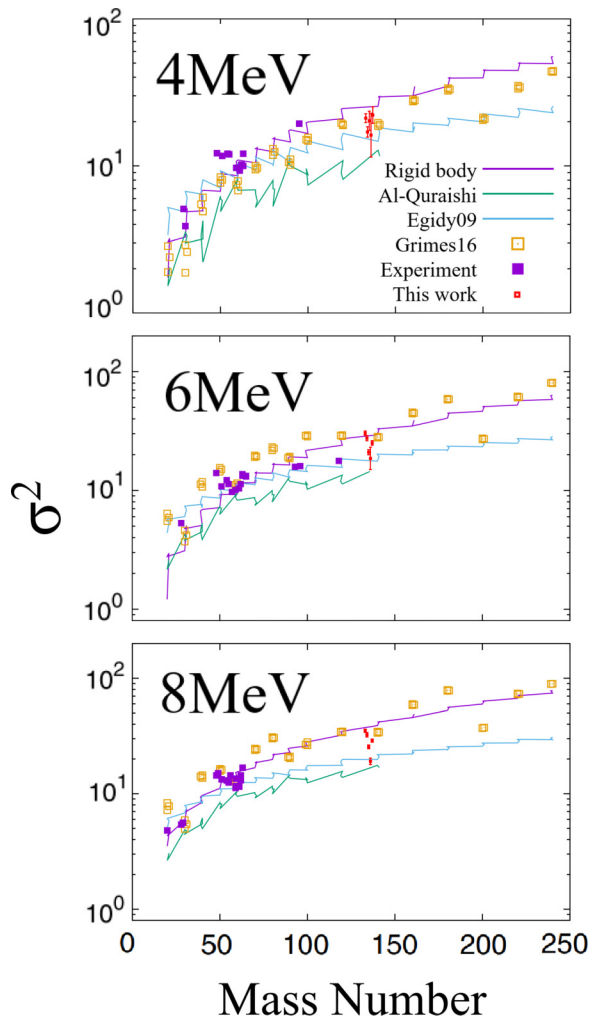
FIG. 15. Spin cut-off parameters for $^{133-137}$Xe (figure adapted from Ref. [69]). The experimental data are taken from Refs. [70,71]. Theoretical results "Al-Quarishi" and "Egidy09" are based on the formula of Ericson [12] with parameters proposed in Refs. [68] and [72], respectively. Theoretical results "Rigid body" and "Grimes16" are from Ref. [69], respectively, based on the rigid-body model and a microscopical method. The theoretical errors of the data in this work originate from the fitting process of the Gaussian distribution.

shell effect. Systematic study showed that σ^2 increases globally with the mass number [72]. However, an abnormal decrease appears near the closed shells [69], which is naturally reproduced by the CISM in the present work. It is also believed that the shell effect is rather important at low excitation energies and becomes weak at energies over the present study ceiling [69].

Another consequence of the shell effect is that σ^2 values for the involved nuclei are larger than the general value derived from the systematic study [72]. The involved nuclei are close to the $N = 82$ shell, while the shell effects are generally neglected in the phenomenological formulas [72]. Recent studies showed that a high-spin structure exists in the nuclei near ^{132}Sn, including Xe [57,74,75] and Ba [76] isotopes. Therefore, the spin cut-off parameter should
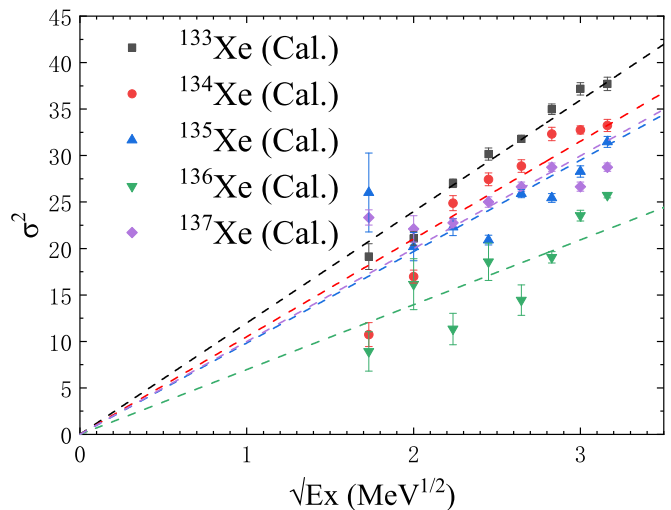

FIG. 16. Energy dependence of spin cut-off parameter in $^{133-137}$Xe. The dashed lines are linear fitting results.

be larger than the predicted values derived without shell effects.

In conclusion, the calculated level-density parity ratio of Xe isotopes demonstrates a distinct odd-even effect at low excitation energy (less than 5 MeV) and tends to 0.5 at high excitation energy, which aligns well with the empirical model presented in Ref. [68]. On the other hand, the spin distribution of Xe isotopes exhibits an odd-even effect for levels lower than 3 MeV, but well follows the Gaussian distribution at higher energies. The derived spin cut-off parameter exhibits a reasonable correspondence with Ref. [69], indicating that its mass dependence at high excitation energy is reasonably described by both the formula of Ericson and the rigid-body model. Meanwhile, the pairing correlation and shell effect contribute to the spin distribution of Xe isotopes near the closed shell, especially at low excitation energies and in even-mass nuclei. The same conclusions can be drawn for Ba isotopes.

IV. SUMMARY

The configuration-interaction shell model (CISM) is employed in the present work to calculate the level density of fission products $^{133-137}$Xe and $^{135-138}$Ba. Five proton orbits and 11 neutron orbits above the core ^{100}Sn constitute the model space, where V_{MU}+LS is used to construct the Hamiltonian. The present Hamiltonian is examined to be suitable in the north vicinity of ^{132}Sn, because it well reproduced both the neutron separation energies of the ground states and the excited energies of low-lying states in nuclei with $Z = 50-56$ and $N \approx 82$.

The stochastic estimation method is used in the present work to calculate the level density. A truncation method based on the monopole interaction is employed to further reduce the computational effort (2–3 orders of magnitude reduction in computational effort). The results of level densities at different energy truncations are compared to determine the suitable truncation energy. The 10 MeV truncation energy is found

to be sufficient to obtain reasonable level-density results in the 0–10 MeV energy range, achieving a balance between calculation dimension and calculation accuracy.

Under such truncation, the results calculated in the present work are consistent with the experimental values of level density at the neutron separation energy and suggest that the cross-shell excitation is more important for the level density calculations for nuclei nearer the $N = 82$ shell gap, $^{135-136}$Xe and $^{137-138}$Ba. The cumulative number of levels in $^{133-137}$Xe and $^{134-138}$Ba at low-excitation energy are generally well reproduced. The proposed method provides a competitive theoretical approach since experimental data are incomplete in the target region.

The effects of the noncentral forces on nuclear level densities are also studied. The results show that the tensor force has a more important influence on the level density than the spin-orbit force. The tensor force enlarges the excitation energy of all the orbits relative to the lowest $0g_{7/2}$ orbits, thus reduces the level density. The spin-orbit force causes the spin-orbit splitting and influences the local level density, but only a slight variation of level density can be seen if the spin-orbit force in the two-body part is removed while its single part remains.

Besides, the parity and spin distributions of $^{133-137}$Xe isotopes are discussed with the empirical formulas. The level densities of different parities are nearly of equal amount at high excitation energies. The calculated spin distributions agree with Eq. (9) at high excitation energy, and deviate from it at low excitation energy where the single-particle effect is significant, especially for the nuclei near the closed shells. Overall, the calculated parity ratios and spin cut-off parameters are consistent with those of empirical models, but provide distinct detailed distribution in some nuclei.

Further investigation of the nuclear forces and more systematic calculations of level density for the fission products are anticipated in future work. On the one hand, the extrapolation ability of the present Hamiltonian is to be verified. On the other hand, it is planned to employ the calculated level density to derive the nuclear reaction data, which are more related to the nuclear engineering and technology application.

[1] Z. Ge and Y. Chen, Sci. Technol. Rev. **39**, 9 (2021).
[2] M. Salvatores, J. Nucl. Sci. Technol. **39**, 4 (2002).
[3] A. J. Plompen, T. Fukahori, H. Henriksson, A. Ignatyuk, T. Iwasaki, G. Manturov, R. D. McKnight, G. Rimpault, and D. L. Smith, *International Conference on Nuclear Data for Scientific Technology* (2007), p. 765.
[4] G. P. Ford, K. Wolfsberg, and B. R. Erdal, Phys. Rev. C **30**, 195 (1984).
[5] S. Hilaire and S. Goriely, Nucl. Phys. A **779**, 63 (2006).
[6] J. Rekstad, A. Henriquez, F. Ingebretsen, G. Midttun, B. Skaali, R. Øyan, J. Wikne, T. Engeland, T. F. Thorstein-sen, E. Hammaren, and E. Liukkonen, Phys. Scr. **T5**, 45 (1983).
[7] A. Schiller, L. Bergholt, M. Guttormsen, E. Melby, J. Rekstad, and S. Siem, Nucl. Instrum. Methods Phys. Res. A **447**, 498 (2000).
[8] A. C. Larsen, M. Guttormsen, M. Krtička, E. Běták, A. Bürger, A. Görgen, H. T. Nyhus, J. Rekstad, A. Schiller, S. Siem, H. K. Toft, G. M. Tveten, A. V. Voinov, and K. Wikan, Phys. Rev. C **83**, 034315 (2011).
[9] A. P. D. Ramirez, A. V. Voinov, S. M. Grimes, A. Schiller, C. R. Brune, T. N. Massey, and A. Salas-Bacci, Phys. Rev. C **88**, 064324 (2013).
[10] S. Goriely, A.-C. Larsen, and D. Mücher, Phys. Rev. C **106**, 044315 (2022).
[11] H. A. Bethe, Rev. Mod. Phys. **9**, 69 (1937).
[12] T. Ericson, Adv. Phys. **9**, 425 (1960).
[13] W. Dilg, W. Schantl, H. Vonach, and M. Uhl, Nucl. Phys. A **217**, 269 (1973).
[14] A. V. Ignatyuk, K. K. Istekov, and G. N. Smirenkin, Sov. J. Nucl. Phys. (Engl. Transl.) **29**, 450 (1979).
[15] T. v. Egidy and D. Bucurescu, Phys. Rev. C **72**, 044311 (2005).
[16] G. H. Lang, C. W. Johnson, S. E. Koonin, and W. E. Ormand, Phys. Rev. C **48**, 1518 (1993).
[17] H. Nakada and Y. Alhassid, Phys. Rev. Lett. **79**, 2939 (1997).
[18] M. G. Mayer, Phys. Rev. **78**, 16 (1950).
[19] J. H. D. Jensen, H. E. Suess, and O. Haxel, Z. Phys. **128**, 295 (1950).
[20] B. A. Brown, Prog. Part. Nucl. Phys. **47**, 517 (2001).
[21] E. Caurier, G. Martínez-Pinedo, F. Nowacki, A. Poves, and A. P. Zuker, Rev. Mod. Phys. **77**, 427 (2005).
[22] T. Otsuka, A. Gade, O. Sorlin, T. Suzuki, and Y. Utsuno, Rev. Mod. Phys. **92**, 015002 (2020).
[23] N. Shimizu, Phys. Lett. B **753**, 13 (2016).
[24] T. Otsuka, T. Suzuki, M. Honma, Y. Utsuno, N. Tsunoda, K. Tsukiyama, and M. Hjorth-Jensen, Phys. Rev. Lett. **104**, 012501 (2010).
[25] G. Bertsch, J. Borysowicz, H. McManus, and W. G. Love, Nucl. Phys. A **284**, 399 (1977).
[26] C. Yuan, T. Suzuki, T. Otsuka, F. Xu, and N. Tsunoda, Phys. Rev. C **85**, 064324 (2012).
[27] Y. Utsuno, T. Otsuka, B. A. Brown, M. Honma, T. Mizusaki, and N. Shimizu, Phys. Rev. C **86**, 051301(R) (2012).
[28] T. Togashi, N. Shimizu, Y. Utsuno, T. Otsuka, and M. Honma, Phys. Rev. C **91**, 024320 (2015).
[29] C. Yuan, Z. Liu, F. Xu, P. Walker, Z. Podolyak, C. xu, Z. Ren, B. Ding, M. Liu, X. Liu, H. Xu, X. Zhou, Y. Zhang, and W. Zuo, Phys. Lett. B **762**, 237 (2016).

[30] C. Yuan, M. Liu, N. Shimizu, Z. Podolyák, T. Suzuki, T. Otsuka, and Z. Liu, Phys. Rev. C **106**, 044314 (2022).

[31] Z. Y. Zhang, H. B. Yang, M. H. Huang, Z. G. Gan, C. X. Yuan, C. Qi, A. N. Andreyev, M. L. Liu, L. Ma, M. M. Zhang, Y. L. Tian, Y. S. Wang, J. G. Wang, C. L. Yang, G. S. Li, Y. H. Qiang, W. Q. Yang, R. F. Chen, H. B. Zhang, Z. W. Lu *et al.*, Phys. Rev. Lett. **126**, 152502 (2021).

[32] H. B. Yang, Z. G. Gan, Z. Y. Zhang, M. H. Huang, L. Ma, M. M. Zhang, C. X. Yuan, Y. F. Niu, C. L. Yang, Y. L. Tian, L. Guo, Y. S. Wang, J. G. Wang, H. B. Zhou, X. J. Wen, H. R. Yang, X. H. Zhou, Y. H. Zhang, W. X. Huang, Z. Liu *et al.*, Phys. Rev. C **105**, L051302 (2022).

[33] C. X. Yuan, Y. L. Ge, M. L. Liu, G. S. Chen, and B. S. Cai, EPJ Web Conf. **239**, 04002 (2020).

[34] C. Yuan and M. Liu (unpublished).

[35] W. E. Ormand and B. A. Brown, Phys. Rev. C **102**, 014315 (2020).

[36] N. Shimizu, arXiv:1310.5431.

[37] R. Takayama, T. Hoshi, T. Sogabe, S. Zhang, and T. Fujiwara, Phys. Rev. B **73**, 165108 (2006).

[38] B. Jegerlehner, arXiv:hep-lat/9612014.

[39] T. Sakurai, Y. Futamura, A. Imakura, and T. Imamura, Scalable eigen-analysis engine for large-scale eigenvalue problems, in *Advanced Software Technologies for Post-Peta Scale Computing: The Japanese Post-Peta CREST Research Project*, edited by M. Sato (Springer Singapore, Singapore, 2019), pp. 37–57.

[40] Y. M. Zhao and A. Arima, Phys. Rep. **545**, 1 (2014).

[41] T. Otsuka, M. Honma, T. Mizusaki, N. Shimizu, and Y. Utsuno, Prog. Part. Nucl. Phys. **47**, 319 (2001).

[42] A. Umeya and K. Muto, Phys. Rev. C **74**, 034330 (2006).

[43] C. X. Yuan, C. Qi, and F. R. Xu, Nucl. Phys. A **883**, 25 (2012).

[44] C. Qi, L. Y. Jia, and G. J. Fu, Phys. Rev. C **94**, 014312 (2016).

[45] M. Wang, W. Huang, F. Kondev, G. Audi, and S. Naimi, Chinese Phys. C **45**, 030003 (2021).

[46] http://www.nndc.bnl.gov/nudat2/.

[47] B. Mottelson, Rev. Mod. Phys. **48**, 375 (1976).

[48] H.-K. Wang, K. Kaneko, and Y. Sun, Phys. Rev. C **89**, 064311 (2014).

[49] H.-K. Wang, K. Kaneko, and Y. Sun, Phys. Rev. C **91**, 021303(R) (2015).

[50] T. Kröll and K. Wimmer, First Spectroscopy of the r-Process Nucleus ^{135}Sn, Technical Report (2018).

[51] G. S. Simpson, G. Gey, A. Jungclaus, J. Taprogge, S. Nishimura, K. Sieja, P. Doornenbal, G. Lorusso, P.-A. Söderström, T. Sumikama, Z. Y. Xu, H. Baba, F. Browne, N. Fukuda, N. Inabe, T. Isobe, H. S. Jung, D. Kameda, G. D. Kim, Y.-K. Kim *et al.*, Phys. Rev. Lett. **113**, 132502 (2014).

[52] H.-K. Wang, Y. Sun, H. Jin, K. Kaneko, and S. Tazaki, Phys. Rev. C **88**, 054310 (2013).

[53] H.-K. Wang, K. Kaneko, Y. Sun, Y.-Q. He, S.-F. Li, and J. Li, Phys. Rev. C **95**, 011304(R) (2017).

[54] H.-K. Wang, Z.-H. Li, C.-X. Yuan, Z.-Q. Chen, N. Wang, W. Qin, and Y.-Q. He, Chin. Phys. C **43**, 054101 (2019).

[55] H.-K. Wang, S. K. Ghorui, K. Kaneko, Y. Sun, and Z. H. Li, Phys. Rev. C **96**, 054313 (2017).

[56] E. Teruya, N. Yoshinaga, K. Higashiyama, and A. Odahara, Phys. Rev. C **92**, 034320 (2015).

[57] A. Vogt, B. Birkenbach, P. Reiter, A. Blazhev, M. Siciliano, K. Hadyńska-Klęk, J. J. Valiente-Dobón, C. Wheldon, E. Teruya, N. Yoshinaga, K. Arnswald, D. Bazzacco, M. Bowry, A. Bracco, B. Bruyneel, R. S. Chakrawarthy, R. Chapman, D. Cline, L. Corradi, F. C. L. Crespi *et al.*, Phys. Rev. C **95**, 024316 (2017).

[58] B. A. Brown, N. J. Stone, J. R. Stone, I. S. Towner, and M. Hjorth-Jensen, Phys. Rev. C **71**, 044317 (2005).

[59] R. Capote, M. Herman, P. Obložinský, P. Young, S. Goriely, T. Belgya, A. Ignatyuk, A. Koning, S. Hilaire, V. Plujko, M. Avrigeanu, O. Bersillon, M. Chadwick, T. Fukahori, Z. Ge, Y. Han, S. Kailas, J. Kopecky, V. Maslov, G. Reffo *et al.*, Nucl. Data Sheets **110**, 3107 (2009).

[60] S. Goriely, S. Hilaire, and A. J. Koning, Phys. Rev. C **78**, 064307 (2008).

[61] N. Fotiades, R. O. Nelson, M. Devlin, J. A. Cizewski, J. A. Becker, W. Younes, R. Krücken, R. M. Clark, P. Fallon, I. Y. Lee, A. O. Macchiavelli, T. Ethvignot, and T. Granier, Phys. Rev. C **75**, 054322 (2007).

[62] T. v. Egidy and D. Bucurescu, J. Phys.: Conf. Ser. **338**, 012028 (2012).

[63] C. X. Yuan, M. L. Liu, and Y. Ge, Nucl. Phys. Rev. **37**, 447 (2020).

[64] H. K. Toft, A. C. Larsen, U. Agvaanluvsan, A. Bürger, M. Guttormsen, G. E. Mitchell, H. T. Nyhus, A. Schiller, S. Siem, N. U. H. Syed, and A. Voinov, Phys. Rev. C **81**, 064311 (2010).

[65] A. Schiller, E. Algin, L. A. Bernstein, P. E. Garrett, M. Guttormsen, M. Hjorth-Jensen, C. W. Johnson, G. E. Mitchell, J. Rekstad, S. Siem, A. Voinov, and W. Younes, Phys. Rev. C **68**, 054326 (2003).

[66] U. Agvaanluvsan, A. C. Larsen, M. Guttormsen, R. Chankova, G. E. Mitchell, A. Schiller, S. Siem, and A. Voinov, Phys. Rev. C **79**, 014320 (2009).

[67] E. Melby, L. Bergholt, M. Guttormsen, M. Hjorth-Jensen, F. Ingebretsen, S. Messelt, J. Rekstad, A. Schiller, S. Siem, and S. W. Ødegård, Phys. Rev. Lett. **83**, 3150 (1999).

[68] S. I. Al-Quraishi, S. M. Grimes, T. N. Massey, and D. A. Resler, Phys. Rev. C **67**, 015803 (2003).

[69] S. M. Grimes, A. V. Voinov, and T. N. Massey, Phys. Rev. C **94**, 014308 (2016).

[70] S. M. Grimes, J. D. Anderson, J. W. McClure, B. A. Pohl, and C. Wong, Phys. Rev. C **10**, 2373 (1974).

[71] P. Hille, P. Sperr, M. Hille, K. Rudolph, W. Assmann, and D. Evers, Nucl. Phys. A **232**, 157 (1974).

[72] T. von Egidy and D. Bucurescu, Phys. Rev. C **80**, 054310 (2009).

[73] T. von Egidy and D. Bucurescu, Phys. Rev. C **78**, 051301(R) (2008).

[74] A. Vogt, B. Birkenbach, P. Reiter, A. Blazhev, M. Siciliano, J. J. Valiente-Dobón, C. Wheldon, D. Bazzacco, M. Bowry, A. Bracco, B. Bruyneel, R. S. Chakrawarthy, R. Chapman, D. Cline, L. Corradi, F. C. L. Crespi, M. Cromaz, G. de Angelis, J. Eberth, P. Fallon *et al.*, Phys. Rev. C **93**, 054325 (2016).

[75] A. Astier, M.-G. Porquet, C. Theisen, D. Verney, I. Deloncle, M. Houry, R. Lucas, F. Azaiez, G. Barreau, D. Curien, O. Dorvaux, G. Duchêne, B. J. P. Gall, N. Redon, M. Rousseau, and O. Stézowski, Phys. Rev. C **85**, 054316 (2012).

[76] L. Coraggio, A. Covello, A. Gargano, N. Itaco, and T. T. S. Kuo, Phys. Rev. C **80**, 044320 (2009).